Available online at www.sciencedirect.com

SciVerse ScienceDirect

Procedia Engineering 00 (2016) 000–000

Procedia Engineering

www.elsevier.com/locate/procedia

1st International Conference on the Material Point Method, MPM 2017

Modeling of liquefaction using two-phase FEM with UBC3D-PLM model

Elizaveta Wobbes[a,*], Lars Beuth[b], Cornelis Vuik[a], Dieter Stolle[c]

[a]*Delft University of Technology, Mekelweg 4, 2628 CD Delft, The Netherlands*
[b]*Deltares, Boussinesqweg 1, 2629 HV Delft, The Netherlands*
[c]*McMaster University, 1280 Main Street West, Hamilton, ON L8S 4L8, Canada*

Abstract

Soil liquefaction describes a loss of strength of saturated sand upon sudden or cyclic loading. A slight disturbance of such a soil's fabric might lead to severe damage, e.g. the collapse of sea dikes. Accurate modeling of the state transition between saturated soil and a liquefied soil-water mixture, as well as post-liquefaction phenomena, is crucial for the prediction of such damage. However, developing an appropriate numerical model remains a challenging problem, especially when the simulation involves dynamic large deformation processes. In order to make a first step towards an accurate simulation of soil liquefaction, a two-phase formulation of the finite element method (FEM) in conjunction with the elastoplastic UBC3D-PLM model is investigated. The performance of this approach is analyzed based on a shaking table benchmark.

Peer-review under responsibility of the organizing committee of the 1 st International Conference on the Material Point Method.

Keywords: MPM; elastoplastic model; liquefaction; cyclic loading.

1. Introduction

Upon sudden or cyclic loading of loose, fully saturated sands, the pore water pressure can rapidly increase leading to a reduction of the mean effective stress. Liquefaction occurs when a state of zero effective stress is reached, thereby eliminating shear strength. The resulting loss of soil strength can induce substantial damages, such as the failure of earth embankments and retaining structures. For instance, liquefaction in the Hanshin and Awaji island district in Japan in 1995 caused by the Kobe earthquake resulted in widespread lateral displacement of the ground, normal faulting, compression ridges, and the generation of quick sand [1]. The cost of ground failure-related damage to the Port of Kobe is estimated at US$10 billion [2]. A more recent example is severe lateral ground movement in Christchurch (New Zealand) in 2010 and 2011 [3]. Due to the high vulnerability to flooding in low-lying countries such as the Netherlands [4], liquefaction of dike or dune sections poses a serious socio-economic threat.
Accurate modeling of the state transition from saturated soil to a liquid sand-water mixture and post-liquefaction phenomena is necessary for the prediction and possible prevention of damages inflicted by liquefaction. This requires

* Corresponding author.
E-mail address: e.d.wobbes@tudelft.nl

Peer-review under responsibility of the organizing committee of the 1 st International Conference on the Material Point Method.

a continuum approach capable of capturing the complex two-phase dynamic behaviour of soil during the process of strength reduction. Additionally, the method should be able to accommodate the large deformations of soil in its liquefied state.

In this paper, a two-phase finite element method (FEM) which is a part of the advanced three-dimensional material point method (MPM) software Anura3D [5,6] is considered together with the UBC3D-PLM model developed by Plaxis [7]. The UBC3D-PLM model is a three-dimensional generalization of the widely known two-dimensional UBCSAND model [8–10]. In [11] it is demonstrated that the UBC3D-PLM model has great potential for modeling of liquefaction-related phenomena.

The performance of the proposed approach is examined by applying the numerical model to a shaking table problem that is based on the well-documented case study in [10]. Despite the complexity of the liquefaction process, the considered example can be reduced to a one-dimensional problem. The simplicity and comprehensive description of this benchmark make it perfectly suited for validation and development of the presented approach.

Currently this study does not include large deformations. However, it provides a firm basis for the development of accurate models for soil state transition. To the authors' knowledge, it is also the first attempt to use the UBC3D-PLM model with the FEM featuring a velocity-based two-phase formulation. In future research, the FEM will be replaced by a "two-point" ("double-point") MPM. The MPM introduced in [12] is an appropriate numerical tool for modeling complex large-deformation problems in continuum mechanics. In this method, the material is represented by a set of Lagrangian particles (material points) that move through a fixed Eulerian mesh. The material points carry the physical properties of the continuum such as mass, strain and stress. With the two-point MPM, the soil skeleton and pore water are represented by different sets of particles [13,14]. Therefore, it can be used for the simulation of the relative motion of sand and water, which is essential for modeling post-liquefaction processes such as landslides, flow slides and soil solidification.

The paper is structured as follows. In Section 2, a brief description of the numerical model is provided. In Section 3, the shaking table benchmark is introduced. Moreover, this section gives an overview of the corresponding input parameters and an analytical solution for the linear elastic version of the problem used to design the mesh. The simulation results are discussed in Section 4. In Section 5, conclusions are drawn.

2. Numerical model

Here, the main aspects of the considered numerical approach are described. In the velocity-based, two-phase formulation the velocities of water and solid phase are the principal unknowns. They are computed from the conservation of momentum equations for water and sand-water mixture, respectively. The momentum equations are:

$$\begin{aligned} \rho_w \frac{dv_{w,i}}{dt} &= \frac{\partial p}{\partial x_i} - \rho_w g_i - \frac{n\gamma_w}{k_i}(v_{w,i} - v_{s,i}), \\ (1-n)\rho_s \frac{dv_{s,i}}{dt} &= -n\rho_w \frac{dv_{w,i}}{dt} + \frac{\partial \sigma_{ij}}{\partial x_j} - \rho_{sat} g_i, \end{aligned} \tag{1}$$

where ρ_w is the water density, $v_{w,i}$ is a component of the velocity vector of the water phase in the i-direction, p is the pore water pressure, g_i is a component of the gravitational acceleration vector in the i-direction, n is the porosity, γ_w is the unit weight of the fluid, k_i is the hydraulic conductivity of soil in the i-direction, $v_{s,i}$ is a component of the velocity vector of the solid phase in the i-direction, ρ_s is the density of the solid phase, σ_{ij} is the total stress tensor, and ρ_{sat} is the saturated density.

For two-phase analysis, the total stress is defined as:

$$\sigma_{ij} = \sigma'_{ij} + p\delta_{ij}, \tag{2}$$

in which σ'_{ij} and δ_{ij} are the effective stress tensor and Kronecker delta, respectively.

The pore pressure rate is then obtained from the storage equation representing the conservation of mass:

$$\frac{\partial p}{\partial t} = \frac{K_w}{n}\left((1-n)\frac{\partial v_{s,i}}{\partial x_i} + n\frac{\partial v_{w,i}}{\partial x_i}\right), \tag{3}$$

where K_w is the bulk modulus of the water phase.
The effective stress rate is computed using the UBC3D-PLM model. The main features of this model are discussed in Section 2.1. To discretize the momentum equations in space the classical finite element approach is adopted for the resulting system of coupled partial differential equations. The semi-implicit Euler-Cromer method is used for the time discretization. For further details the reader is referred to [15,16].

2.1. Constitutive relation

2.1.1. Elastic behaviour

In the UBC3D-PLM model, the elastic component of the response is determined by the elastic shear modulus, G^e, and the elastic bulk modulus, B^e, in the following way:

$$\begin{aligned} G^e &= k_G^e P_A \left(\frac{p'}{P_A}\right)^{n_G}, \\ B^e &= k_B^e P_A \left(\frac{p'}{P_A}\right)^{n_B}. \end{aligned} \tag{4}$$

Here, k_G^e and k_B^e are, respectively, the shear and bulk moduli numbers, P_A is the atmospheric pressure, p' is the mean effective stress, n_G and n_B are the elastic exponents defining the dependence of stiffness on stress.
Purely elastic behaviour is predicted upon unloading, which is characterized by a decrease in the magnitude of the stress ratio.

2.1.2. Plastic behaviour

Plastic strains are generated during first time loading and reloading. They are controlled by primary and secondary yield surfaces. First time loading occurs when the stress ratio exceeds the highest stress ratio in the loading history. In this case the primary yield surface based on isotropic hardening is activated. As the magnitude of the stress ratio increases, the yield surface is "dragged" to a new location, expanding the elastic region. Unloading deactivates the primary yield surface. During reloading the current stress ratio does not exceed the previous stress ratio limits and the model produces less plastic strains when compared to first time loading. This is achieved by using a kinematic hardening rule for the secondary yield surface which is activated upon reloading. Both yield surfaces are defined by the Mohr-Coulomb yield function given by:

$$f_m = \frac{1}{2}\left(\sigma'_{max} - \sigma'_{min}\right) - \left(\frac{1}{2}\left(\sigma'_{max} + \sigma'_{min}\right) + c\cot\phi_p\right)\sin\phi_{mob}, \tag{5}$$

where σ'_{max} and σ'_{min} are, respectively, the maximum and minimum principal effective stresses, c is the cohesion, ϕ_p is the peak friction angle, and ϕ_{mob} is the mobilized friction angle.
The plastic potential function is based on the Drucker-Prager model and can be expressed as follows:

$$g_m = q - \frac{6\sin\psi_{mob}}{3 - \sin\psi_{mob}}\left(p' + c\cot\phi_p\right), \tag{6}$$

where q is the deviatoric stress and ψ_{mob} is the mobilized dilation angle. The mobilized dilation angle is computed from ϕ_{mob} and the constant volume friction angle, ϕ_{cv}, in the following manner:

$$\sin\psi_{mob} = \sin\phi_{mob} - \sin\phi_{cv}. \tag{7}$$

The hardening rule introduced in [8] is:

$$d\sin\phi_{mob} = 3k_G^p\left(\frac{p'}{P_A}\right)^{np}\frac{P_A}{\sigma'_{max} + \sigma'_{min}}\left(1 - \frac{\sin\phi_{mob}}{\sin\phi_p}R_f\right)^2 d\lambda, \tag{8}$$

where k_G^p is the plastic shear modulus number, np is the plastic shear modulus exponent, R_f is the failure ratio and $d\lambda$ is the plastic shear increment.

During first time loading k_G^p is equal to k_{G0}^p, which is an input parameter. However, upon secondary loading it is replaced by the updated plastic shear modulus:

$$k_{Gi}^p = k_{G0}^p \left(4 + \frac{n_{rev}}{2}\right) k_{dens} fac_{dens}. \tag{9}$$

Here, n_{rev} is the number of shear stress reversals from loading to unloading and vice versa, k_{dens} is a factor between 0.5 and 1.0 required to correct the densification rule and fac_{dens} is a densification factor extracted after curve fit.

3. Shaking table benchmark

In the shaking table benchmark, a 38 m high column of loose, fully saturated sand is considered. The bottom of the column is impermeable and subjected to an acceleration of $0.2g \sin(3\pi t)$. Centrifuge tests presented in [10] were carried out at Rensselaer Polytechnic Institute (RPI) for a scaled-down column. These experiments were performed using a laminar box consisting of rings which were allowed to move laterally, parallel to the direction of shearing. The laboratory results are compared with numerical data obtained with a finite difference method utilizing the UBCSAND model for a prototype-scale benchmark referred to as RPI model 1 [10]. The complexity of the numerical analysis was elegantly reduced to a one-dimensional representation of the problem by making the following assumptions. First of all, each horizontal layer was allowed to change its volume in the vertical direction and undergo shear deformation due to horizontal shear stress, while compression and expansion in the horizontal direction were prohibited. In addition, uniform strains and stresses along every horizontal plane were assumed. Figure 1 illustrates the experimental and numerical setups considered in [10].

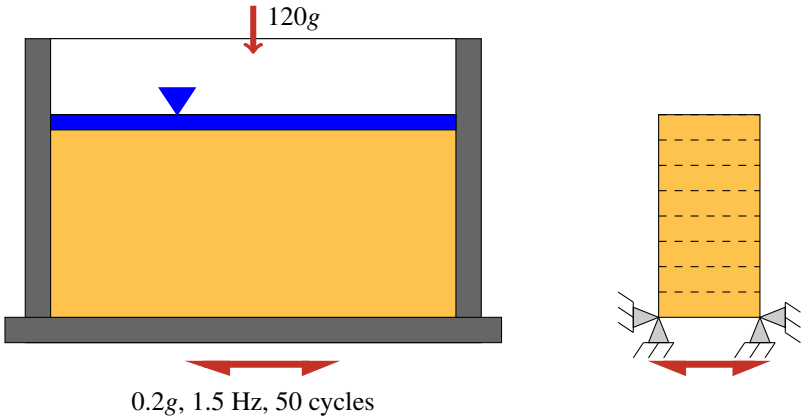

Fig. 1. Shaking table benchmark: schematic representation of experimental (left) and numerical (right) setups.

In this paper the motion of the column is studied with respect to its bottom surface. For this reason, the dynamic boundary condition is replaced by an inertial force according to d'Alembert's principle [17]. Mathematically, this modification is equivalent to the substitution of horizontal displacement $u(y,t)$ with $w(y,t)$ defined as:

$$w(y,t) = u(y,t) + \frac{0.2g}{9\pi^2} \sin(3\pi t). \tag{10}$$

Moreover, the grid nodes located on the same horizontal plane are tied in order to enforce the one-dimensional representation of the three-dimensional discretization of the column.

3.1. Input parameters

Since the benchmark can be reduced to a one-dimensional problem, the size of the column base is not relevant and is, therefore, set to 1 m × 1 m. A homogeneous soil column is assumed. Table 1 provides the input parameters for the model. These values are based on the information provided in [10,18–20] for Nevada sand fully saturated with water.

Table 1. Input parameters.

Parameter	Soil column	Parameter	Soil column
Initial porosity [-]	0.40	Elastic bulk modulus number [-]	1067
Density solid [kg/m^3]	2600	Elastic shear modulus exponent [-]	0.50
K0-value [-]	0.50	Elastic bulk modulus exponent [-]	0.50
Intrinsic permeability liquid [m^2]	$6.97 \cdot 10^{-12}$	Plastic shear modulus exponent [-]	0.50
Young's modulus [N/m^2]	$2.50 \cdot 10^8$	Failure ratio [-]	0.95
Poisson ratio [-]	0.20	Atmospheric pressure [Pa]	$1.00 \cdot 10^5$
Cohesion [N/m^2]	0	Densification factor [-]	0.50
Constant volume friction angle [°]	31	Density liquid [kg/m^3]	1000
Peak friction angle [°]	32	Bulk modulus liquid [N/m^2]	$0.60 \cdot 10^8$
Elastic shear modulus number [-]	800	Dynamic viscosity liquid [Pa·s]	$1.00 \cdot 10^{-6}$
Plastic shear modulus number [-]	500	Gravitational acceleration [m/s^2]	10

3.2. Mesh

In order to determine the required level of mesh resolution, preliminary simulations are performed with a linear elastic stress-strain relation. This simplified model admits an analytical solution for this benchmark. The solution is given by:

$$w(y,t) = \sum_{n=1,3,5,\ldots} A_n(t) \sin\left(\frac{\pi n y}{2H}\right), \tag{11}$$

where H is the column height and A_n is a time-dependent coefficient defined as:

$$A_n(t) = -\frac{3.2 g \rho H^2}{n\pi^3 \left(n^2 G - 36\rho H^2\right)} \left(\sin(3\pi t) - \frac{6H}{n\sqrt{G/\rho}} \sin\left(\frac{n\pi\sqrt{G/\rho}}{2H} t\right)\right). \tag{12}$$

The column is discretized into 38 layers of size 1 m × 1 m × 1 m. Each layer consists of six tetrahedral elements with one material point in the center of each element. Figure 2 demonstrates nearly exact agreement between the displacements at the beginning of the simulation. After 1 s the relative L_2 error is equal to $4.37 \cdot 10^{-4}$ m. Although after 30 s the relative error increases to $3.05 \cdot 10^{-2}$ m due to the time-stepping error, the figure depicts considerable similarity between the numerical solution and the analytical data at the end of the simulation. It is concluded that the mesh is sufficiently fine for this numerical study.

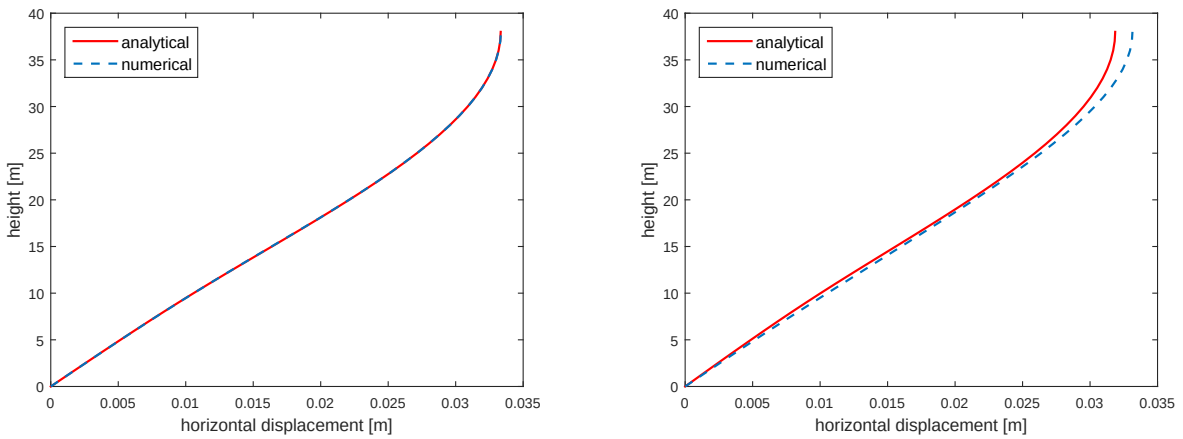

Fig. 2. Analytical and numerical solutions for linear elastic shaking table problem after 1 s (left) and 30 s (right).

4. Results

In this section, the results obtained from the shaking table case study with a two-phase FEM in conjunction with the UBC3D-PLM model are discussed. Figure 3 displays the initial mean effective stress and pore pressure distributions over the column height, as well as the distributions after 2.5 s, 5 s, 10 s, 20 s, 30 s and 40 s after the beginning of the simulation.

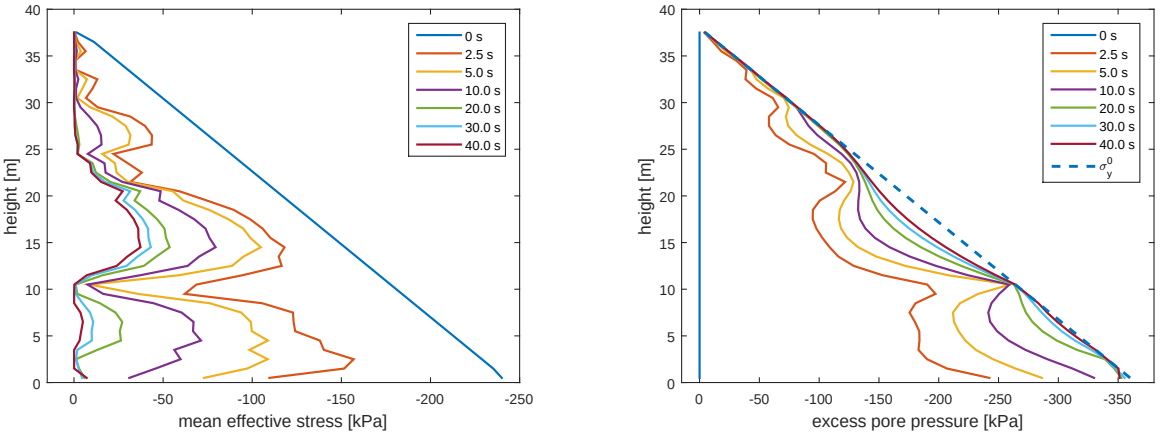

Fig. 3. Mean effective stress (left) and pore pressure (right) distribution over column height after 0 s, 2.5 s, 5 s, 10 s, 20 s, 30 s and 40 s.

Before shaking, the magnitude of the mean effective stress increases with depth according to:

$$p'(y,0) = \frac{(1+2K_0)}{3}\rho_{sub}g(H-y). \tag{13}$$

Here, p' is the mean effective stress, y is the height level, K_0 is the coefficient of lateral earth pressure, ρ_{sub} is the submerged soil density, and H is the total height of the column.

After 2.5 s of cyclic loading, the mean effective stress becomes zero at the top of the column indicating local liquefaction. The magnitude of the excess pore water pressure along the whole column increases significantly. The pore pressure growth is accompanied by oscillations at $y = 10$ m and $y = 22$ m.

As the shaking continues, a top-down trend of the strength loss develops in the top part of the soil column, i.e. liquefaction occurs first near the surface and then propagates downward. However, after 5 s, the model predicts near-liquefaction at a height of 10.5 m. This is an unexpected result, because the magnitude of the mean effective stress in the main part of the column above this level is significantly larger.

After 30 s, the upper 14 m of the column have completely liquefied and the near-liquefaction state is identified at the bottom of the column, from $y = 0$ m to $y = 12$ m. In the middle part of the column the mean effective stress is limited to -44 kPa. Following [10], the shaking is terminated at 33.3 s, while the simulation is continued until 40 s. At the end of the simulation, excess pore pressure approaches the initial vertical effective stress distribution which implies that total effective stress is vanishing.

In Figure 4 the numerical results are compared to experimental data extracted from [10]. The figure underlines the observed merits and drawbacks of the approach adapted in this paper by illustrating the excess pore pressure time history at different heights. At a height of 24.9 m the model predicts the soil behaviour with adequate accuracy. Near the bottom surface, at $y = 1.0$ m, the initial growth of the pore pressure magnitude is faster than during the laboratory experiment. However, after 15 s, the model depicts the liquefaction process correctly. At a height of 13.2 m, the liquefaction process is significantly slower compared to measurements.

The early liquefaction of the bottom layers of the column was observed in the numerical analysis of [10] as well. Initially the finite difference model predicted a bottom-up liquefaction trend. The simulation results followed the top-down trend detected in the experiments after the soil density was increased with depth. It is expected that density adjustment would improve the results obtained with the FEM approach. In addition, the detected deviations might be

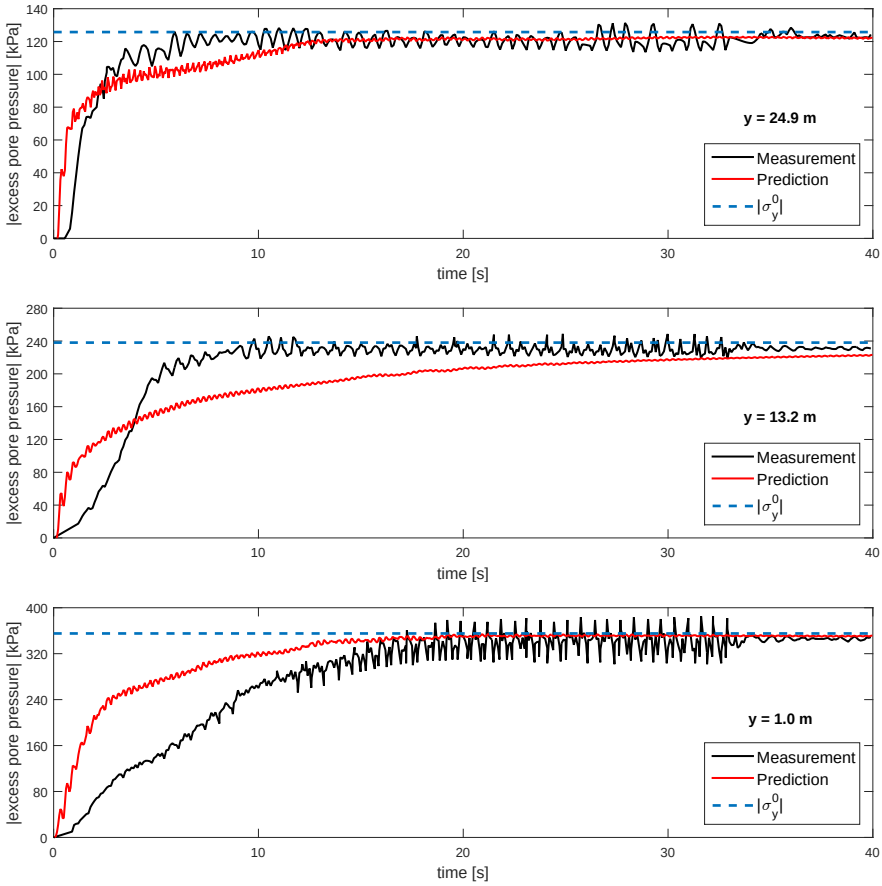

Fig. 4. Measured [10] and predicted excess pore pressure at y = 1.0 m, y = 13.2 m and y = 24.9 m.

reduced by further calibration of the UBC3D-PLM model parameters. For instance, the value of plastic shear modulus has a strong influence on the oscillatory behaviour of stresses.

5. Conclusions

The objective of this preliminary study was to model soil liquefaction using a two-phase formulation of the FEM in conjunction with the UBC3D-PLM constitutive model. The approach was tested on a shaking table benchmark describing shear loading of a 38 m high column of loose saturated sand. The model prediction was compared with experimental data reported in [10]. The results demonstrated that the FEM combined with an elaborate elastoplastic constitutive equation was capable of simulating the shear-induced change of mean effective stress. The proposed approach also partially reproduced the top-down liquefaction trend. It is expected that further calibration of the model and adjustment of soil density with depth would render a closer fit to the experiments. In future research, this benchmark will be used for validation and enhancement of the recently developed two-point MPM.

Acknowledgments

This study was carried out as a part of the MPM-Flow project “Understanding flow slides in flood defences” in collaboration with Utrecht University. The project is funded by the Dutch Technology Foundation (STW), Deltares, Royal Boskalis Westminster N.V., Van Oord Dredging and Marine Contractors, Rijkswaterstaat and Stichting IJkdijk.

The authors are grateful to Plaxis for providing access to the UBC3D-PLM digital library, and Vahid Galavi for his suggestions, criticism and encouragement.

References

[1] Y. Miyachi, K. Kimura, A. Sangawa, Liquefaction and the associated lateral migration of the Hanshin district in the 1995 Hyogoken-Nanbu earthquake (Kobe earthquake), Central Japan, Engineering Geology 23 (1997) 409–422.
[2] S. E. Chang, Disasters and transport systems: loss, recovery and competition at the Port of Kobe after the 1995 earthquake, Journal of Transport Geography 8 (2000) 53–65.
[3] M. Cubrinovski, K. Robinson, M. Taylor, M. Hughes, R. Orense, K. Robinson, M. Taylor, M. Hughes, R. Orense, Lateral spreading and its impact in urban areas in the 2010-2011 Christchurch earthquakes, New Zealand Journal of Geology and Geophysics 55 (2012) 255–269.
[4] S. van Baars, I. van Kempen, The causes and mechanisms of historical dike failures in the Netherlands, E-WAter (2009) 1–14.
[5] A. Rohe, A. Yerro Colom, MPM Software-Anura3D, Technical Report May, 2016.
[6] I. Jassim, D. Stolle, P. A. Vermeer, Two-phase dynamic analysis by material point method, International Journal for Numerical and Analytical Methods in Geomechanics 37 (2013) 2502–2522.
[7] A. Petalas, V. Galavi, R. B. J. Brinkgreve, Validation and verification of a practical constitutive model for predicting liquefaction in sands (2012) 1–6.
[8] H. Puebla, P. M. Byrne, R. Phillips, Analysis of CANLEX liquefaction embankments: prototype and centrifuge models, Canadian Geotechnical Journal 34 (1997) 641–657.
[9] M. Beaty, P. M. Byrne, An effective stress model for predicting liquefaction behaviour of sand, Geotechnical Special Publication 1 (1998) 766–777.
[10] P. M. Byrne, S. Park, M. Beaty, M. Sharp, L. Gonzalez, T. Abdoun, Numerical modeling of liquefaction and comparison with centrifuge tests, Canadian Geotechnical Journal 41 (2004) 193–211.
[11] V. Galavi, A. Petalas, R. B. J. Brinkgreve, Finite element modelling of seismic liquefaction in soils, Geotechnical Engineering 44 (2013) 55–64.
[12] D. Sulsky, Z. Chen, H. L. Schreyer, A particle method for history-dependent materials, Computer Methods in Applied Mechanics and Engineering 118 (1994) 179–196.
[13] S. Bandara, K. Soga, Coupling of soil deformation and pore fluid flow using material point method, Computers and Geotechnics 63 (2015) 199–214.
[14] P. A. Vermeer, L. Sittoni, L. Beuth, Z. Wieckowski, Modeling soil-fluid and fluid-soil transitions with applications to tailings, in: Tailings and Mine waste, 2013, pp. 305–315.
[15] I. K. J. AL-Kafaji, Formulation of a dynamic material point method (MPM) for geomechanical problems, Ph.D. thesis, Stuttgart University, 2013.
[16] M. M. J. Mieremet, Numerical stability for velocity-based 2-phase formulation for geotechnical dynamic analysis, Master's thesis, Delft University of Technology, 2015.
[17] R. W. Clough, J. Penzien, Dynamics of structures, Technical Report, 1975.
[18] R. S. Steedman, R. H. Ledbetter, M. E. Hynes, The influence of high confining stress on the cyclic behaviour of saturated sand, in: Soil Dynamics and Liquefaction 2000, American Society of Civil Engineers, Denver, Colorado, United States, 2000.
[19] K. Arulmoli, K. K. Muraleetharan, M. M. Hossain, L. S. Fruth, VELACS verification of liquefaction analyses by centrifuge studies laboratory testing program soil data report, Technical Report, National Science Foundation, Washington, D.C., 1992.
[20] A. B. Tsegaye, Liquefaction Model (UBC3D), Technical Report, Plaxis B.V., Delft, 2010.